Optimization of Four-Button BPM Configuration for Small-Gap Beam Chambers*

S. H. Kim

Advanced *Photon Source*
Argonne National Laboratory
9700 South Cass Avenue
Argonne, Illinois 60439 USA

Abstract. The configuration of four-button beam position monitors (BPMs) employed in small-gap beam chambers is optimized from 2-D electrostatic calculation of induced charges on the button electrodes. The calculation shows that for a narrow chamber of width/height (w/h) >> 1, over 90% of the induced charges are distributed within a distance of 2h from the charged beam position in the direction of the chamber width. The most efficient configuration for a four-button BPM is to have a button diameter of (2–2.5)h with no button offset from the beam. The button sensitivities in this case are maximized and have good linearity with respect to the beam positions in the horizontal and vertical directions. The button sensitivities and beam coefficients are also calculated for the 8 mm and 5 mm chambers used in the insertion device straight sections of the 7 GeV Advanced Photon Source.

INTRODUCTION

Circular button electrodes are commonly used as beam position monitors (BPMs) in a variety of particle accelerators (1, 2). For highly relativistic filamentary beams of electrons or positrons, the Lorentz contraction compresses the electromagnetic field of the charged beam into the 2-D transverse plane. This results in the induced currents on the beam chamber wall having the same longitudinal intensity modulation as the charged beam. When the wavelength of the beam intensity modulation is large compared to the button diameters, the calculation of the induced charges on the buttons may be simplified as a 2-D electrostatic problem. In the insertion device (ID) straight sections of the 7 GeV positron storage ring for the Advanced Photon Source (APS), beam chambers 8 mm and 5 mm in height are used to optimize the ID magnetic parameters. In this paper the configuration of four-button BPMs in a small-gap beam chamber is optimized, and BPM sensitivities and coefficients are calculated assuming that the button electrodes are flush with the chamber wall.

* Work supported by the U.S. Department of Energy, Office of Basic Energy Sciences under Contract No. W-31-109-ENG-38.

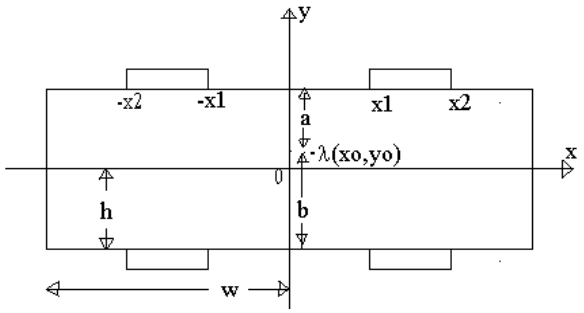

FIGURE 1. Cross section of a beam chamber with a height of 2h and width of 2w. The diameter of the four button electrodes for the BPM system is $(x_2 - x_1)$, and $b = h + y_o$, $a = h - y_o$.

IMAGE CHARGES

Assuming that the width of the beam chamber in Figure 1 is much larger than the height (w >> h), the induced charges are calculated by the method of image charge. The beam chamber is also assumed to have a high electric conductivity and is grounded. Then the vertical positions of the positive and negative image charges of a charge λ at (x_o, y_o) are given by

$+\lambda$ at $y = 2m(a+b) + y_o = 4mh + y_o$, $(m = -\infty, 0, \infty)$

and $-\lambda$ at $y = 2a + 2m(a + b) + y_o = 2a + 4mh + y_o$(for integer m, $-\infty<m<\infty$) (1)

with $a = h-y_o$ and $b = h+y_o$. For ease of calculation the vertical position for $(-\lambda)$ is shifted by $2h$ so that $y' = y-2h = 4mh - y_o$. (In the 3-D geometry the charge λ is a line-charge density along the z direction.) Then the electrostatic potential distribution $\Phi(x,y)$ within the chamber may be calculated from

$$\frac{-\lambda}{2\pi\varepsilon_0}\ln\frac{|z-z_o|\prod_{m=1}^{\infty}|(z-z_m)(z-z_{-m})|}{|z'-z'_o|\prod_{m=1}^{\infty}|(z'-z'_m)(z'-z'_{-m})|} = \Phi(x,y) = \frac{-\lambda}{2\pi\varepsilon_0}\ln\frac{\prod_{m=-\infty}^{\infty}|z-z_m|}{\prod_{m=-\infty}^{\infty}|z'-z'_m|}, \qquad (2)$$

where ε_0 is the permittivity in free space, $z = x + i\,y$, $z' = x + i\,y'$, $z_{-m} = x_o + i\,(-4mh+y_o)$, and $z'_{-m} = x_o + i\,y' = x_o + i\,(-4mh-y_o)$. Equation (2) may be simplified to a closed form

$$\Phi(x,y) = \frac{-\lambda}{2\pi\varepsilon_0}\,\mathrm{Re}\left\{\ln\frac{\sin\pi(\frac{z-x_o-iy_o}{4hi})}{\sin\pi(\frac{z'-x_o+iy_o}{4hi})}\right\}$$

$$= \frac{-\lambda}{4\pi\varepsilon_0}\ln\frac{\cosh\pi\frac{x-x_o}{2h}-\cosh\pi\frac{y-y_o}{2h}}{\cosh\pi\frac{x-x_o}{2h}+\cosh\pi\frac{y-y_o}{2h}} \qquad (3)$$

where y' is shifted back to $y + 2h$ in the final expression.

The induced charge densities per x/h in the top and bottom surfaces of the chamber, σ_t and σ_b, are calculated from $[-\varepsilon_o\, d\Phi/dy]_{y=-h}$

$$\sigma_t = -\frac{\lambda}{4}\frac{\cos py_o}{\cosh p(x-x_o)-\sin py_o},$$

$$\sigma_b = -\frac{\lambda}{4}\frac{\cos py_o}{\cosh p(x-x_o)+\sin py_o}. \qquad (4)$$

Here $p = \pi/2$ and by setting $h = 1$ the coordinate system is normalized to the half height of the chamber. By adding up the induced charges in the top and bottom surfaces in Equation (4), the total induced charge, which should be proportional to the sum signal for a typical four-button BPM system of Figure 1, is given by

$$Q_s = Q_s(x_2) - Q_s(x_1) = \int_{x1}^{x2}(\sigma_t+\sigma_b)dx + \int_{-x2}^{-x1}(\sigma_t+\sigma_b)dx$$

$$= -\lambda\frac{1}{2}\int_{x1}^{x2}\{\frac{\cos py_o\cosh p(x-x_o)}{\cosh^2 p(x-x_o)-\sin^2 py_o}+\frac{\cos py_o\cosh p(x+x_o)}{\cosh^2 p(x+x_o)-\sin^2 py_o}\}dx. \qquad (5)$$

The induced charges proportional to the signals for the vertical and horizontal positions of the charged beam, Q_y and Q_x, may be calculated from Equation (4):

$$Q_y = Q_y(x_2) - Q_y(x_1) = \int_{x1}^{x2}(\sigma_t-\sigma_b)dx + \int_{-x2}^{-x1}(\sigma_t-\sigma_b)dx, \qquad (6)$$

$$Q_x = Q_x(x_2) - Q_x(x_1) = \int_{x1}^{x2}(\sigma_t+\sigma_b)dx - \int_{-x2}^{-x1}(\sigma_t+\sigma_b)dx. \qquad (7)$$

Here Q_y and Q_x are the differences in the induced charges between the top and bottom, and right and left buttons, respectively. As one expects from beam position measurements, Q_y is an odd function in y_o and even in x_o, and Q_x is the opposite. After Taylor expansions up to the third order in the charged beam position (x_o, y_o), indefinite integrals of Equations (5–7) are given by

$$\frac{Q_s(x)}{-\lambda} = \frac{1}{p}\tan^{-1}[\sinh px] + (y_o{}^2 - x_o{}^2)\frac{p\sinh px}{2\cosh^2 px} + y_o{}^2 x_o{}^2 \frac{p^3}{4}\left(\frac{\sinh px}{\cosh^2 px} - \frac{6\sinh px}{\cosh^4 px}\right), \quad (8)$$

$$\frac{Q_y(x)}{-\lambda} = y_o[\tanh px + x_o{}^2 p^2 \frac{-\sinh px}{\cosh^3 px}] + y_o{}^3[p^2 \frac{\sinh px}{3\cosh^3 px}$$

$$+ x_o{}^2 p^4\left(\frac{2\sinh px}{3\cosh^3 px} - \frac{2\sinh px}{\cosh^5 px}\right)], \quad (9)$$

$$\frac{Q_x(x)}{-\lambda} = x_o[-\sec h(px) + y_o{}^2 p^2\{\frac{1}{2}\sec h(px) - \sec h^3(px)\}] + x_o{}^3[\frac{p^2}{6}\{2\sec h^3(px)$$

$$-\sec h(px)\} + y_o{}^2 p^4\{2\sec h^5(px) - \frac{5}{3}\sec h^3(px) + \frac{1}{12}\sec h(px)\}]. \quad (10)$$

To the first order in y_o/h and x_o/h, calculations of the induced charges from $x_1 = 0$ to $x_2 = \infty$ in Equations (8–10) give $Q_y = -\lambda y_o/h$, $Q_x = -\lambda x_o/h$, and the total induced charge $Q_s = -\lambda$ as expected. The derivatives of $Q_s(x)$, $Q_y(x)$, and $Q_x(x)$ with respect to x/h may be called "the effective induced charge densities for the sum, vertical, and horizontal signals." The first terms of the charge densities and Equations (8–10) are plotted in Figure 2.

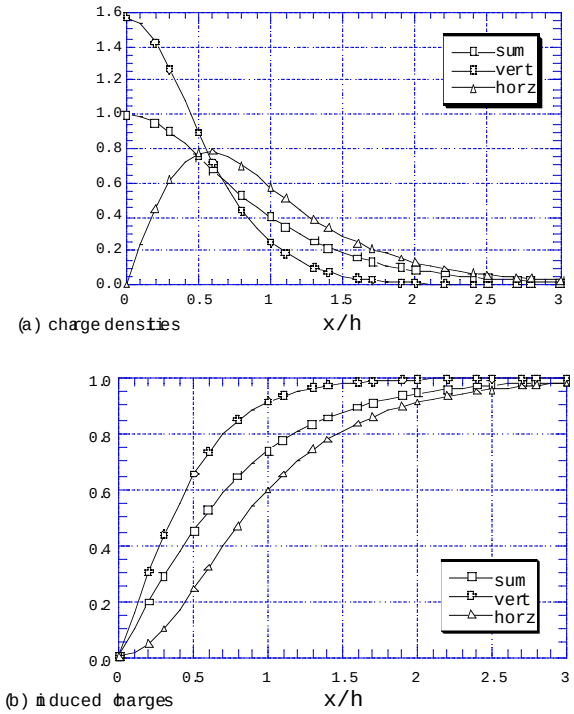

FIGURE 2. (a) Induced charge densities and (b)induced charges integrated from 0 to x/h. The induced charges and densities corresponding to Q_s, Q_y, and Q_x in Equation (8) are denoted as sum, vert, and horz in the legends, respectively, with units of $-\lambda$, $-\lambda y_o/h$, and $-\lambda x_o/h$.

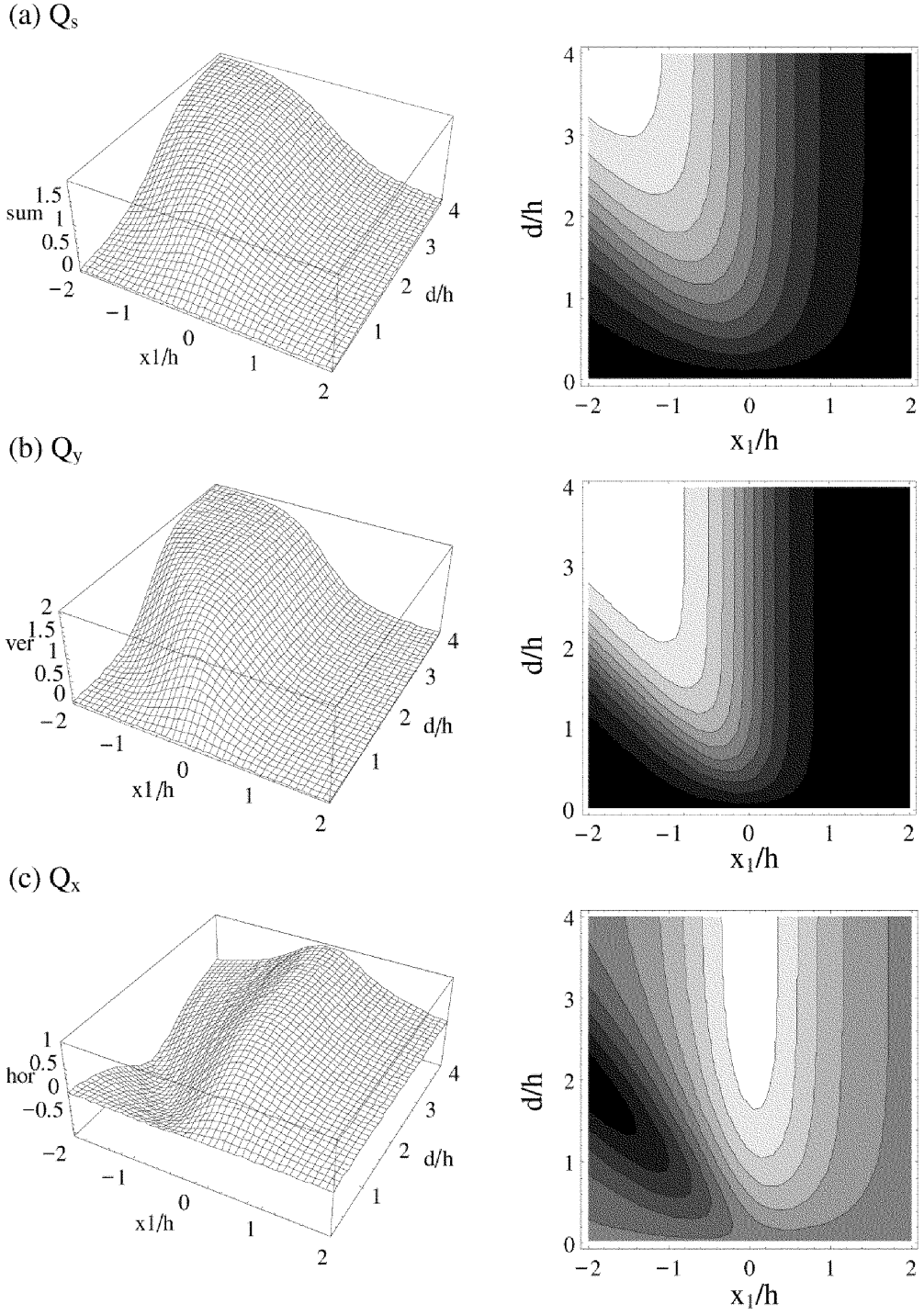

FIGURE 3. 3-D plots of the induced charges for Q_s, Q_y, and Q_x as functions of normalized button offset x_1/h and button diameter d/h on the left side, and their contour plots on the right side. The respective units for Q_s, Q_y, and Q_x are $-\lambda$, $-\lambda y_o/h$, and $-\lambda x_o/h$.

For small buttons (e.g., $x/h < 0.5$), when the beam is located near the origin, the horizontal beam displacement is not as sensitive to changes in the distances between the beam and the buttons as the vertical beam displacement. This makes the density distribution for Q_x broad with the peak near $x/h = 0.6$. The density for Q_y, on the other hand, has its peak at $x/h = 0$. This implies that, when the measurements of vertical displacements are critical for a beam chamber of small height, the location of the buttons should include the range of small x/h. For buttons located in the range of $x = 0 - 2h$ with button diameter of $2h$, for example, over 94%, 99%, and 91% of the available sensitivities for sum, vertical, and horizontal can be registered on the buttons. Therefore, any buttons located more than $2h$ (one chamber height) from the beam position in the horizontal direction would be very inefficient.

Shown in Figure 3 are 3-D plots and their contours for Q_s, Q_y, and Q_x. The negative position of x_1 is possible by rotating the four-button system with respect to the vertically symmetrical axis. For $x_1 = 0$ and a button diameter d larger than $2h$, it is seen that Q_s, Q_y, and Q_x do saturate as already expected from Figure 2. When the buttons are extended to both sides of the x-axis by rotating the four-button system and the diameter is larger than $4h$, the values of Q_s and Q_y increase by a factor of 2 because most parts of the buttons are still located within $x/h < 2$ where the charge densities are high. On the other hand, Q_x decreases because the charge density for Q_x is asymmetric with respect to x. Therefore, a four-button system with a button diameter of approximately $(2\sim2.5)h$ and a button offset of $x_1 = 0$ would collect nearly all the induced charges and be the most efficient.

BUTTON SENSITIVITIES

With $x_1 = 0$ and $d = 2h$, where the button diameter d is $(x_2 - x_1)h$, Q_s, Q_y, Q_x, and their normalized values to Q_s are calculated from Equations (5–7). The results give an optimized BPM configuration and are plotted in Figure 4 as functions of the normalized beam position $(y_o/h, x_o/h)$. The button sensitivities and coefficients for y_o/h and x_o/h for the optimized configuration are calculated from Equations (8–10).

Optimized configuration:

$$Q_s = 0.945[1.0 + 0.07143\ \{(y_o/h)^2 - (x_o/h)^2\} + 0.0842\ (x_o/h)^2(y_o/h)^2],$$

$$Q_y = 0.9963[\{1.0 - 0.01836\ (x_o/h)^2\}(y_o/h) + \{0.00612 + 0.0295\ (x_o/h)^2\}(y_o/h)^3,$$

$$Q_x = 0.9137[\{1.0 + 1.4649\ (y_o/h)^2\}(x_o/h) - \{0.4883 + 2.7354\ (y_o/h)^2\}(x_o/h)^3],$$

$$Q_y/Q_s = 1.0542[\{1 + 0.0531\ (x_o/h)^2\}(y_o/h) - \{0.0653 + 0.0631\ (x_o/h)^2\}(y_o/h)^3],$$

$$Q_x/Q_s = 0.9669[\{1 + 1.3935\ (y_o/h)^2\}(x_o/h) - \{0.4169 + 2.6159\ (y_o/h)^2\}(x_o/h)^3]. \quad (11)$$

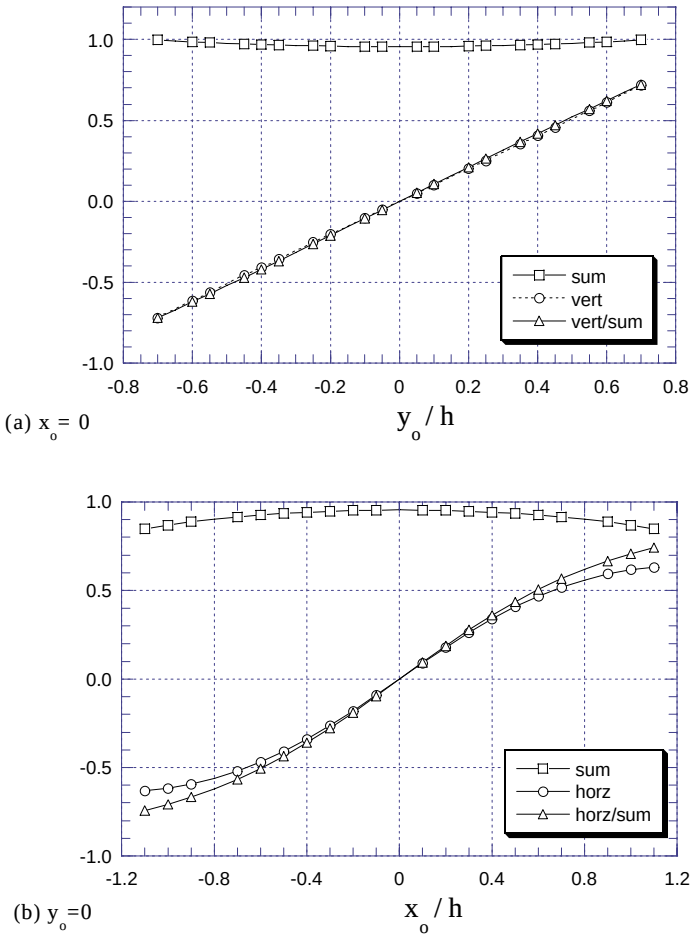

FIGURE 4. For the optimized BPM configuration, normalized button positions of $x_1/h = 0$and $x_2/h = 2$ (normalized diameter $d/h = 2$), variations (a) Q_s, Q_y, and Q_y/Q_s are plotted as a function of normalized vertical beam position y_o/h for $x_o = 0$, and (b) Q_s, Q_x, and Q_x/Q_s as a function of normalized horizontal beam position x_o/h for $y_o = 0$. Here Q_s, Q_y, and Q_x are denoted as sum, vertical, and horizontal and their respective units are $-\lambda$, $-\lambda y_o/h$, and $-\lambda x_o/h$.

Figure 4(a) and Equation (11) show that the vertical signals Q_y and Q_y/Q_s within $-0.7y_o/h$ have excellent linearity in y_o/h and x_o/h. This is particularly important since vertical measurements are generally critical in a small chamber height. The horizontal signals Q_x and Q_x/Q_s, on the other hand, are less linear compared to those for the vertical as seen from Figure 4(b) and the coefficients of y_o/h and x_o/h in Equation (11).

In the APS storage ring, beam chambers with relatively small chamber heights are used for the IDs in the straight sections (3). Several four-button BPMs with button diameters of 4 mm and button-center separations of 9.65 mm have been installed for chamber heights of 8 mm (h = 4 mm, $x_1 = 0.7075h$, $x_2 = 1.7075h$, diameter = $1.0h$) and 5 mm (h = 2.5 mm, $x_1 = 1.132h$, $x_2 = 2.732h$, diameter = $1.6h$). One can see from Figure 2 that these buttons are located at relatively inefficient positions compared to the optimized case of $x_1 = 0$ and $x_2 = 2h$. The button sensitivities and y_o and x_o coefficients for the two chambers are:

APS ID chamber (2h = 8 mm):

$$Q_s = 0.3178[1.0 + 0.0529\ \{x_o^2 - y_o^2\} + 0.00778\ x_o^2 y_o^2],$$

$$Q_y = 0.0465[\{1.0 + 0.2199\ x_o^2\}\ y_o + \{-0.0733 + 0.00228\ x_o^2\} y_o^3,$$

$$Q_x = 0.1144[\{1.0 - 0.00738\ y_o^2\}\ x_o + \{0.00246 + 0.00827\ y_o^2\} x_o^3],$$

$$Q_y/Q_s = 0.1464\ [\{1 + 0.1669\ x_o^2\}\ y_o + \{- 0.2033 + 0.00502\ x_o^2\}\ y_o^3],$$

$$Q_x/Q_s = 0.360\ [\{1 + 0.0456\ y_o^2\}\ x_o + \{-0.5049 + 0.00229\ y_o^2\}\ x_o^3]. \qquad (12)$$

The smallest aperture APS chamber (2h = 5 mm):

$$Q_s = 0.1957[1.0 + 0.1817\ \{x_o^2 - y_o^2\} - 0.0104\ x_o^2 y_o^2],$$

$$Q_y = 0.02205[\{1.0 + 0.7246\ x_o^2\}\ y_o - \{0.2415 + 0.1285\ x_o^2\} y_o^3,$$

$$Q_x = 0.1205[\{1.0 - 0.1509\ y_o^2\}\ x_o + \{0.0503 + 0.0136\ y_o^2\} x_o^3],$$

$$Q_y/Q_s = 0.1127\ [\{1 + 0.5429\ x_o^2\}\ y_o - \{0.0598 + 0.00858\ x_o^2\}\ y_o^3],$$

$$Q_x/Q_s = 0.6156\ [\{1 + 0.0308\ y_o^2\}\ x_o - \{0.1314 + 0.0146\ y_o^2\}\ x_o^3]. \qquad (13)$$

As seen from Equations (12) and (13), the most critical signals Q_y for 8 mm and 5 mm chambers are only 0.046 and 0.022 of the unit $-\lambda y_o/h$. Compared to Q_y, the horizontal signals Q_x are over 0.11 of the unit $-\lambda x_o/h$ for both chambers. Even if the normalized signals are not too small (because of the small values of Q_s), one should expect that the noise/signal ratios for Q_y/Q_s and Q_x/Q_s in Equations (12) and (13) are relatively large compared to those in Equation (11).

ACKNOWLEDGMENTS

The author would like to thank Glenn Decker for his numerous suggestions and useful discussions concerning this work.

REFERENCES

[1] Shafer, R. E., "Beam Position Monitoring," presented at the First Accelerator Instrumentation Workshop, Upton, NY, Oct. 23–26, 1989, *AIP Conference Proceedings* **212**, 26-58 (1989).

[2] Barry, W. C., "Broad-Band Characteristics of Circular Button Pickups," *Proceedings of the Fourth Accelerator Instrumentation Workshop*, Berkley, CA, Oct. 27-30, 1992, *AIP Conference Proceedings,* **281**, 175–184 (1993).

[3] Lumpkin, A. H., "Commissioning Results of the APS Storage Ring Diagnostics System," *Proceedings of the Seventh Accelerator Instrumentation Workshop, Argonne,* IL, May 6-9, 1996, *AIP Conference Proceedings*, **390**, 152–172 (1997).